Journal of Nuclear Materials 399 (2010) 32–37

Contents lists available at ScienceDirect

Journal of Nuclear Materials

journal homepage: www.elsevier.com/locate/jnucmat

Effect of ion irradiation and indentation depth on the kinetics of deformation during micro-indentation of Zr–2.5%Nb pressure tube material at 25 °C

B. Bose, R.J. Klassen *

Department of Mechanical and Materials Engineering, Faculty of Engineering, University of Western Ontario, London, Ontario, Canada N6A 5B9

ARTICLE INFO

Article history:
Received 20 October 2009
Accepted 28 December 2009

ABSTRACT

Micro-indentation creep tests were performed at 25 °C on radial-normal samples cut from Zr–2.5Nb CANDU pressure tube material in both the as-fabricated condition and after irradiation with 8.5 MeV Zr^+ ions. The average indentation stress, and hence the yield stress, was found to increase with decreasing indentation depth and with increasing levels of ion irradiation. The activation energy of the indentation creep rate and hence the, activation energy of the obstacles that limit the rate of dislocation glide, was independent of indentation depth but increased from $\Delta G_0 = 0.185$ to 0.215 μb^3 with increasing ion irradiation damage. The magnitude of the activation energy indicates that ion irradiation introduces a new type of obstacle into the microstructure which reduces the low temperature indentation creep rate of Zr–2.5Nb pressure tubes. This is supported by TEM images showing that Zr^+ ion irradiation produces small, nanometer size, dislocation loops which act as obstacles to dislocation glide and thus influence both the yield stress and the activation energy of the low-temperature thermal creep of Zr–2.5Nb pressure tube material. These findings suggest that neutron irradiation will have similar effect upon yield stress and low-temperature thermal creep as the Zr^+ ion irradiation since both create similar crystallographic defects in Zr–2.5Nb pressure tubes.

© 2010 Elsevier B.V. All rights reserved.

1. Introduction

Zr–2.5Nb pressure tubes have proven to be very reliable components of the fuel-channel assemblies of CANadian Deuterium Uranium (CANDU) nuclear reactors however the inside surface of these tubes can become scratched during service and the local stress ahead of these scratches can be high enough to require the early removal of a pressure tube from the reactor core. It is therefore necessary to be able to predict the local creep rate ahead of sharp scratches on the inside surface of these pressure tubes in order to make accurate flaw assessments. While the thermal creep characteristics of Zr–2.5Nb pressure tube material at low applied stress levels have been reported [1,2] the creep rate under high magnitude multi-axial stress conditions and the effect of neutron irradiation hardening on the thermal creep rate has not been thoroughly studied. The research presented in this paper uses pyramidal micro-indentation creep tests performed at 25 °C to simulate the creep rate ahead of a scratch on the inside surface of a Zr–2.5Nb CANDU pressure tube. The effect of indentation depth and ion irradiation hardening (as a simulation of neutron irradiation hardening) on the mechanism of indentation creep deformation is investigated. Some important underlying principles pertaining to this investigation are described below.

1.1. Indentation creep tests to simulate creep at scratches

Scratches on the inside surface of CANDU pressure tubes, arising from refueling operations and rubbing between fuel bundle bearing pads and the inside wall of the pressure tube, often have similar depth and sharpness to pyramidal micro-indentations. Pyramidal micro-indentation creep tests therefore offer a way to simulate the creep deformation around such scratches. Constant-force micro- and nano-indentation creep tests have been used to study the kinetics of plastic deformation of a variety of materials [3–9] and the results of such tests are usually interpreted in terms of deformation occurring by a mechanism of dislocation glide limited by discrete obstacles distributed throughout the microstructure [10,11]. Most of the published indentation creep investigations were performed on relatively isotropic material (i.e. fcc metals). The kinetics of high-stress low-temperature indentation creep of mechanically anisotropic materials, such as the extruded and cold-drawn Zr–2.5Nb pressure tube alloy, has not been reported. This information is not only important for understanding the fundamentals of the indentation creep process but is also important for establishing basic kinetic parameters that can be used in expressions describing the creep rate of material around

* Corresponding author. Tel.: +1 519 661 2111x88323; fax: +1 519 661 3020.
E-mail address: rklassen@eng.uwo.ca (R.J. Klassen).

0022-3115/$ - see front matter © 2010 Elsevier B.V. All rights reserved.
doi:10.1016/j.jnucmat.2009.12.019

scratches that have geometrical similarities to pyramidal indentations.

1.2. Mechanism of creep deformation ahead of scratches in Zr–2.5Nb pressure tubes

The combination of very high equivalent stress at the tip of a crack, or surface flaw, in a Zr–2.5Nb pressure tube and the fact that the service temperature of the tube is low relative to the solidus temperature (T/T_{melt} = 0.14–0.17) suggests that thermal creep ahead of the sharp scratches occurs by a mechanism of dislocation glide at a rate limited by the interaction of the gliding dislocations with discrete obstacles in the microstructure. When deformation occurs by such a mechanism the shear strain rate $\dot{\gamma}$ can be expressed in terms of the yield shear stress τ_{yield}, the effective shear stress τ_{eff} driving the creep process, and the absolute temperature T as [10]

$$\dot{\gamma} = \dot{\gamma}_p \left(\frac{\tau_{yield}}{\mu}\right)^2 e^{-\frac{\Delta G(\tau_{eff})}{kT}} \quad (1)$$

where $\dot{\gamma}_p$ is a constant (approximately equal to 10^{11} s^{-1} [10]), μ is the elastic shear modulus, k is Boltzmann's constant and $\Delta G(\tau_{eff})$ is the thermal energy required for a dislocation, subjected to τ_{eff}, to overcome the discrete obstacles. The following general expression for $\Delta G(\tau_{eff})$ has been proposed [10,11]

$$\Delta G(\tau_{eff}) = \Delta G_0 \left[1 - \left(\frac{\tau_{eff}}{\hat{\tau}}\right)^p\right]^q \quad (2)$$

In this equation ΔG_0 is the activation energy of the discrete obstacles, $\hat{\tau}$ is the athermal flow strength of the material, p and q are constants. ΔG_0 and the constants p and q are characteristic of the particular dislocation–obstacle interaction that governs the creep rate and, in the case of Zr–2.5Nb pressure tubes, may depend upon temperature, indentation depth, and the degree of neutron irradiation hardening. The study described in this paper addresses the dependence of ΔG_0 upon indentation depth and ion irradiation.

1.3. Indentation size effect

The indentation hardness of metals decreases with increasing indentation depth from 0.1 to about 10 μm. The hardness then remains relatively constant with further increasing depth. This depth dependence of the indentation hardness is widely thought to result from the fact that a higher local dislocation density is necessary to accommodate the larger plastic strain gradients associated with sub-micrometer deep indentations [12–17]. While the indentation depth dependence of hardness has been studied extensively for relatively isotropic fcc metals, it has not been thoroughly investigated for mechanically anisotropic metals such as the highly textured Zr–2.5Nb pressure tube alloy. In this study we perform indentation tests at depths from 0.1 to 2.0 μm to assess the indentation size effect on the indentation stress of the extruded and cold-drawn Zr–2.5 Nb pressure tube alloy before and after 1 h indentation creep testing. In so doing we hope to gain insight into the indentation depth dependence of the kinetics of dislocation motion in this material when subjected to high-level multi-axial indentation stress for an extended time at 25 °C.

1.4. Ion irradiation to simulate neutron irradiation

The role of neutron irradiation as a source for the production of point defects and nanometer-scale dislocation loops and the result of these defects on increasing the yield stress of the Zr–2.5Nb alloy is well documented [18–26]. The use of proton- and electron-irradiation to simulate the microstructural damage resulting from neutron irradiation is also widely reported [27–31]. Previous research has shown that heavy ion bombardment of metals results in the creation of crystallographic damage consisting of dislocation loops similar in size and character to that produced, at a slower rate, by neutron irradiation [32,33]. In this study we use Zr^+ irradiation of the Zr–2.5Nb to simulate the microstructural damage resulting from neutron irradiation without causing significant compositional change to the test material.

2. Experimental procedure

2.1. Material

Rectangular samples, 8.5 mm long, 8.5 mm wide and 4.0 mm thick, were cut from a non-irradiated Zr–2.5%Nb CANDU pressure tube. The general chemical composition of this alloy is: 2.5–2.7 wt.% Nb, 1100–1200 ppm O, ~1000 ppm Fe, <55 ppm N, <16 ppm H, and balance Zr [34]. The tube was fabricated by 11:1 extrusion of an annular billet at 720 °C followed by 27% cold-drawing at room temperature followed by a 24 h stress relief autoclave treatment at 400 °C [1,35]. The microstructure of the tube consists of hcp α-Zr grains, elongated in the axial direction of the tube, surrounded by a thin discontinuous layer of Nb-rich bcc β precipitates. The α grains have average dimensions of about 0.2, 1.0 and 5.0 μm in the radial, hoop and axial directions of the pressure tube respectively. The α grains are textured with the majority of the basal plane normals aligned along the hoop direction of the tube [36]. The Radial-Normal (RN) surface, relative to the radial direction of the pressure tube, of each sample was prepared by mechanical grinding and polishing followed by chemical polishing. The average roughness of the final polished surface was about ±8 nm as measured with atomic force microscopy. The RN plane was chosen as the surface upon which to perform the micro-indentation creep tests since it is the same orientation as the inside surface of a Zr–2.5Nb pressure tube and, therefore, the same surface that becomes scratched during service.

2.2. Zr^+ ion irradiation

Some of the polished samples were exposed to 8.5 MeV Zr^+ ions to introduce irradiation damage to the material. The ion irradiation was performed in vacuum in the Tandetron 1.7 MV tandem ion accelerator at the University of Western Ontario (London, ON). Monte Carlo simulations carried out with the SRIM software indicate that the maximum interaction of the Zr^+ ions with the Zr

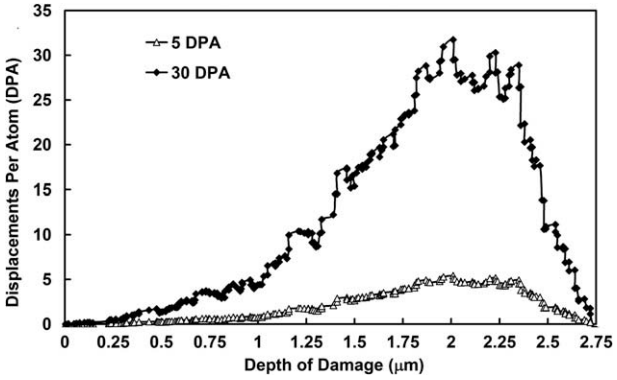

Fig. 1. Calculate irradiation damage, in units of displacement per atom (dpa), resulting from 8.5 MeV Zr^+ ions versus depth in the irradiated Zr 2.5Nb sample. One sample was exposed to a relatively low dosage of Zr^+ ions corresponding to about a maximum of 5 dpa while another group of sample was exposed to a higher dosage corresponding to a maximum of about 30 dpa at a depth of 2.0–2.5 μm.

2.5Nb alloy occurs at a depth between 2.0 and 2.5 μm (Fig. 1). One group of samples was exposed to a relatively low dosage of Zr^+ ions, corresponding to a maximum of about 5 displacements per atom (dpa) at a depth of between 2.0 and 2.5 μm while another group of samples was exposed to a higher dosage corresponding to a maximum damage of about 30 dpa.

2.3. Micro-indentation creep tests

Constant-force Berkovich indentation creep tests were performed at 25 °C on the polished RN surface of the Zr–2.5Nb samples using an instrumented nano-/micro-indentation testing platform made by Micro Materials ltd (Wrexham, UK). Indentation creep tests were carried out at initial indentation depths of h_0 = 0.1, 0.5, 1.0 and 2.0 μm for both the non-irradiated and the ion-irradiated samples. For each test the indentation force (F) was slowly applied until the desired h_0 was reached. F was then held constant for 1 h while the indentation depth h was continuously recorded. Between 7 and 10 indentation creep tests were performed at each h_0 on the non-irradiated, the 5 dpa, and the 30 dpa Zr^+ irradiated samples.

2.4. TEM investigations

Electron transparent foils, of about 500 nm thicknesses, were extracted by focused ion beam (FIB) milling from within the indentation plastic zone of 500 nm deep crept indentations from the non-irradiated and the ion-irradiated samples (Fig. 2). The FIB milling was performed using a LEO XB1540 dual beam FIB/SEM with 30 keV Ga^+ ions of 1nA current. The final 100–150 nm thickness was slowly removed with a Ga^+ ion current of 50 pA. Parallel beam transmission electron microscopy (TEM) was performed on the samples with a PHILIPS CM12 microscope operating at 120 kV.

3. Results and discussion

The average indentation stress σ_{ind} was calculated as:

$$\sigma_{ind} = \frac{F}{24.5Ch^2} \tag{3}$$

where $24.5h^2$ is the projected area of an ideal Berkovich indentation and C is a constant that accounts for the effect of sink-in and pile-up on the projected indentation area. C was obtained from SEM measurement of the projected area of indentations of various depths.

The average indentation strain rate $\dot{\varepsilon}_{ind}$ is related to the instantaneous indentation depth h and indentation velocity $\dot{h}$ as:

$$\dot{\varepsilon}_{ind} = k\left(\frac{\dot{h}}{h}\right) \tag{4}$$

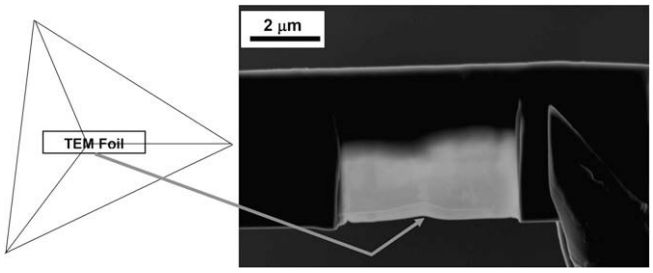

Fig. 2. Schematic illustration of the orientation of a TEM foil extracted, by FIB milling, from an as-crept indentation made in the Zr 2.5Nb test material. The SEM image shows the extracted foil with the profile of the indentation clearly visible beneath the deposited Pt protective later.

where k is a material constant that, due to the geometrical self-similarity of the pyramidal indentation, is independent of h over the depth range considered in this study. Since k remains constant, we set it equal unity and refer to $\dot{\varepsilon}_{ind}$ as the apparent average indentation strain rate.

During the constant-F stage of the micro-indentation tests, h increases with time due to creep deformation and this result in decreasing σ_{ind} (Fig. 3a and b). In Fig. 4 the initial indentation stress $\sigma_{ind_{t=0}}$ is plotted versus the initial indentation depth h_0, prior to creep testing. Power-law functions of indentation depth fitted to the data show that $\sigma_{ind_{t=0}}$ of the Zr–2.5Nb material in this study is a function of both the indentation depth and the level of Zr^+ ion irradiation. Since the strain gradient in the indentation plastic zone increases inversely with the indent size (Section 1.3), σ_{ind} often reaches a magnitude of a few percent of the Young's modulus, i.e. almost the ideal strength of the indented material, when the indentation depth is less than 1 μm. David Tabor has shown that for deep indentations, where indentation size effects are not a factor, σ_{ind} is a function of the uniaxial yield stress for most materials ($\sigma_{ind} \approx 3\sigma_{yield}$ [37]). Using this empirical correlation, $\sigma_{ind_{t=0}}$ from the deepest indentations in our study (depth 2 μm) corresponds to a uniaxial yield stress that is similar in magnitude to the reported value for the cold-worked Zr–2.5Nb pressure tube alloy [38–40].

In Fig. 5 the indentation stress at the end of the constant-F stage, $\sigma_{ind_{t=1\ h}}$ is plotted against the final indentation depth h_f. The plot shows that σ_{ind} at the end of the creep tests, i.e. after

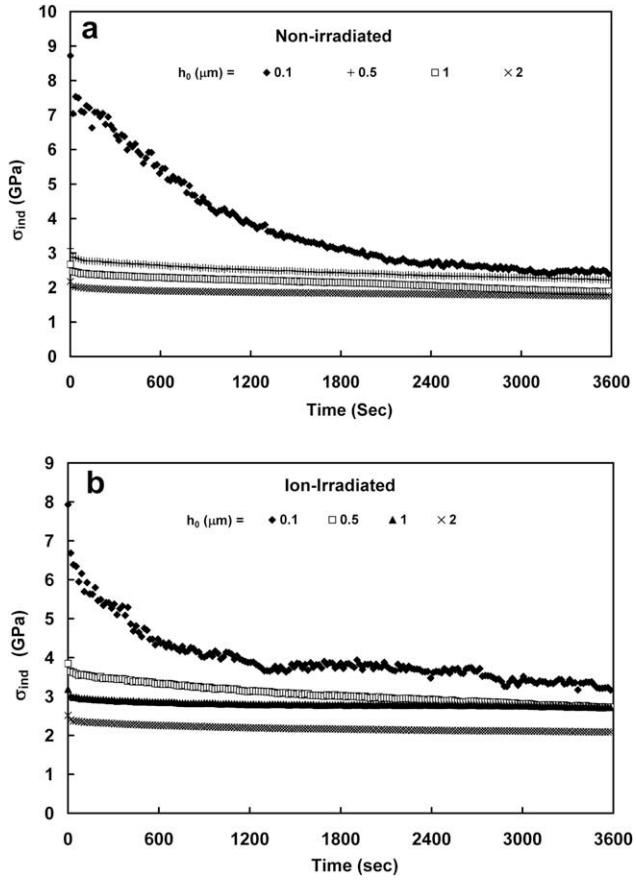

Fig. 3. Typical average indentation stress σ_{ind} versus time plots during the indentation creep tests performed on (a) non-irradiated and (b) 30 dpa Zr^+ irradiated Zr 2.5Nb samples performed at different values of h_0. Although the trend is similar for all samples, the indentation stress σ_{ind} values are higher for the irradiated samples.

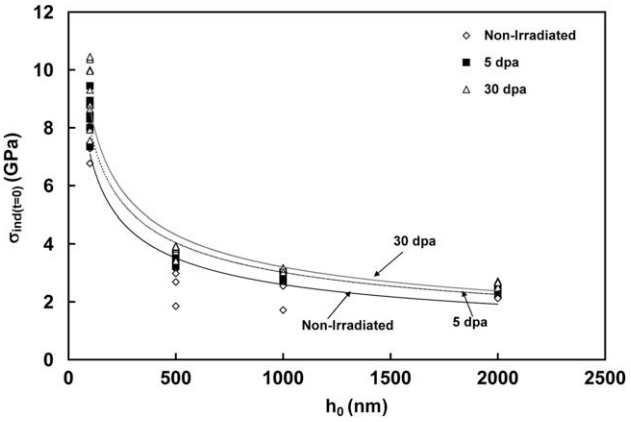

Fig. 4. Variation in initial indentation stress, i.e. indentation stress at the beginning of creep tests, $\sigma_{ind(t=0)}$ with initial indentation depth, h_0 for three different sample conditions (as received, 5 dpa and 30 dpa). $\sigma_{ind(t=0)}$ decreases with h_0 and increases with irradiation damage.

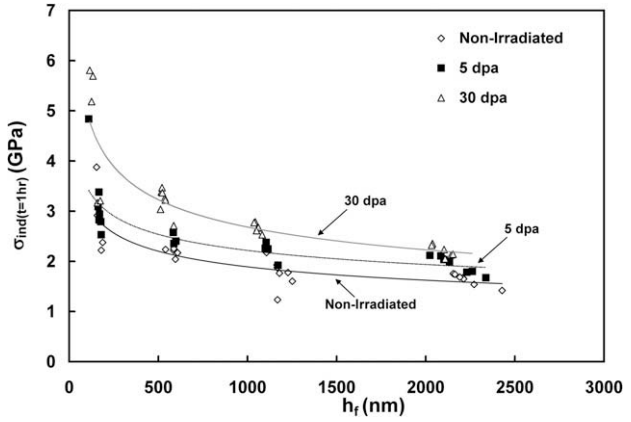

Fig. 5. Indentation stress at the end of the 1 h constant F creep tests $\sigma_{ind_{t=1\ h}}$ versus final indentation depth, h_f plot for the three different sample conditions (as received, 5 dpa and 30 dpa). For all cases the 30 dpa Zr^+ irradiated sample has the highest final indentation stress. The value of $\sigma_{ind_{t=1\ h}}$ also decrease with increasing indentation depth.

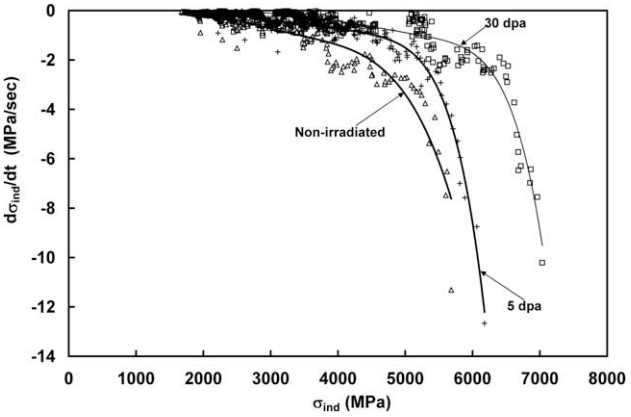

Fig. 6. The rate of change of indentation stress, $\partial\sigma_{ind}(t)/\partial t$, i.e. the slope of the curves in Fig. 3, versus σ_{ind} for the three different sample conditions (as received, 5 dpa and 30 dpa). For all cases the shape of the curve is clearly dependent upon the level of ion irradiation and data from tests performed at different indentation depths lie on essentially the same curves.

significant creep deformation has occurred, still displays dependence upon indentation depth and upon the level of Zr^+ ion irradiation. This suggests that, even after 1 h recovery under constant F conditions, the dislocation density is still higher for the shallow indentation compared to the deep indentation.

Fig. 6 shows a plot of the rate of change of indentation stress, $\partial\sigma_{ind}(t)/\partial t$, i.e. the slope of the curves in Fig. 3, versus σ_{ind}. While the shape of the curves is clearly dependent upon the level of ion irradiation, the data from tests performed at different indentation depths lie on essentially the same curve. This indicates that while the indentation creep behaviour of the material depends upon the level of ion irradiation it is not dependent upon indentation depth over the depth range considered in this study ($0.1\ \mu m < h < 2.0\ \mu m$).

Figs. 7 and 8 show TEM images of the indentation plastic zone of a non-irradiated and a 30 dpa ion irradiated sample. Both samples display elongated α phase grains with high dislocation density that is characteristic of the extrusion/cold-drawing fabrication route of the test material. However, the ion irradiated sample also displays large regions of mottled "salt and pepper" contrast. Previous investigations have shown that small, less than 5 nm diameter, dislocation loops formed in Zr–2.5Nb as a result of electron irradiation at 77 °C [36]. The mottled contrast displayed in Fig. 8 is very likely to be diffraction contrast resulting from a uniform distribution of small dislocation loops resulting from the Zr^+ ion irradiation.

The 1 h constant-force indentation creep tests provide data from which σ_{ind} and $\dot{\varepsilon}_{ind}$ can be calculated as a function of time using Eqs. (3) and (4). We have used these data to determine the following expressions for the equivalent indentation shear stress τ_{ind}, the equivalent effective indentation shear stress τ_{eff} and the apparent equivalent indentation shear strain rate $\dot{\gamma}_{ind}$ [11]:

$$\tau_{ind} = \frac{\sigma_{ind}}{3\sqrt{3}} \quad \tau_{eff} = \frac{\sigma_{ind} - \sigma_{ind_{t=1\ h}}}{3\sqrt{3}} \text{ and } \dot{\gamma}_{ind} = \sqrt{3}\dot{\varepsilon}_{ind} = \frac{\sqrt{3}\dot{h}}{h} \qquad (5)$$

$\Delta G(\tau_{eff})$, the thermal energy required for a dislocation subjected to a shear stress τ_{eff} to overcome an obstacle of strength ΔG_0, was calculated by fitting Eq. (1) to the τ_{ind}, τ_{eff} and $\dot{\gamma}_{ind}$ data (see Fig. 9).

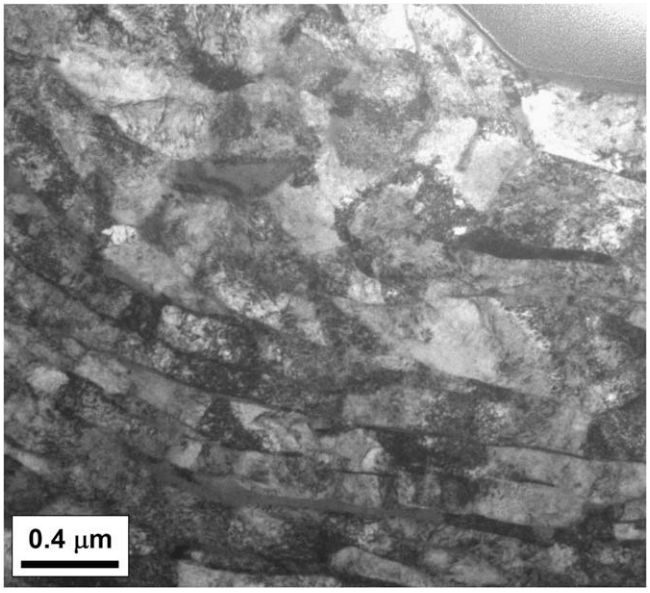

Fig. 7. TEM image of an as-crept indentation plastic zone in the non-irradiated Zr 2.5Nb sample. A very high, but inhomogeneous, dislocation distribution exists everywhere in the sample (including far from the indentation). This dislocation distribution is therefore attributed to the 27% cold drawing stage of the pressure tube fabrication.

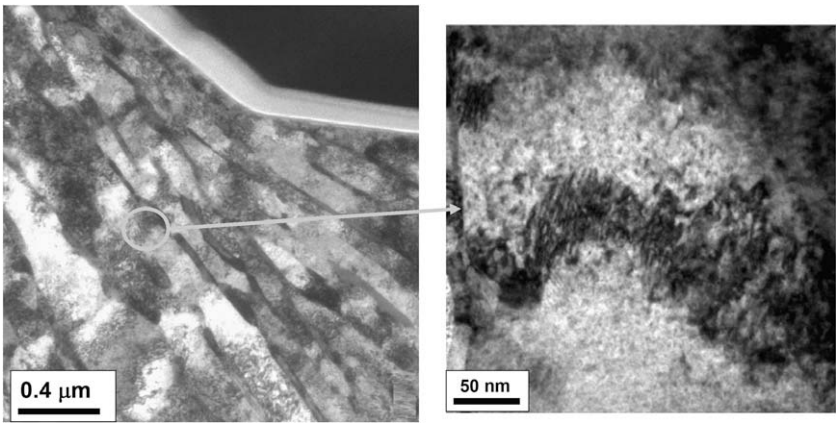

Fig. 8. TEM image of the as-crept indentation plastic zone in a 30 dpa Zr^+ irradiated Zr 2.5Nb sample. The higher magnification inset displays large regions of mottled "salt and pepper" contrast which was not observed in the non-irradiated sample (Fig. 7) and is therefore attributed to diffraction contrast resulting from a uniform distribution of small dislocation loops resulting from the Zr^+ ion irradiation. The sizes of the dislocation loops at room temperature are expected to be less than 5 nm [36].

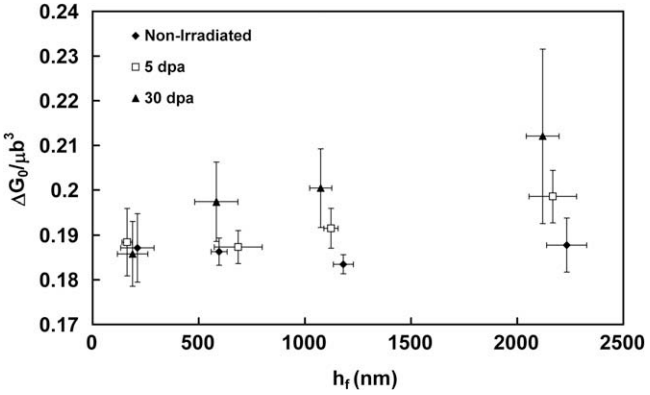

Fig. 9. The activation energy ΔG_0 of the obstacles that limit the rate of indentation creep versus final indentation depth h_f. The error bars represent ± one standard deviation of the measured population (sample size between 7 and 10). ΔG_0 is essentially independent of h_f (within the variability of the measured ΔG_0) however its magnitude increases with increasing Zr^+ irradiation damage.

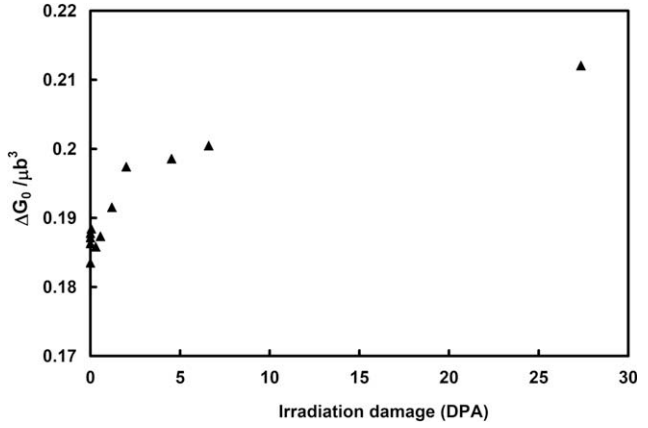

Fig. 10. The activation energy ΔG_0 of the obstacles that limit the rate of indentation creep versus the calculated dpa at the final indentation depth h_f of each test (Table 1). ΔG_0 clearly increases in a non-linear way with increasing degree of Zr^+ ion irradiation damage.

The activation energy ΔG_0 of the obstacles that limit the dislocation glide, and hence the indentation creep rate, was determined by extrapolating the $\Delta G(\tau_{eff})$ versus τ_{eff} trends obtained from each indentation creep test to $\tau_{eff} = 0$. Fig. 10 shows ΔG_0 plotted as a function of final indentation depth h_f. ΔG_0 does not change with indentation depth for the non-irradiated sample. This is in agreement with what has been previously reported for ΔG_0 of Au and Al alloys during indentation creep at 25 °C [5,6]. If one considers the data from a specific indentation depth ΔG_0 increases with increasing ion irradiation damage. The dependence of ΔG_0 upon irradiation damage is shown clearly in Fig. 10 where the average ΔG_0 data from all the tests performed on the Zr^+ ion irradiated material are plotted versus the calculated dpa level corresponding to the final indentation depth h_f (Table 1). The TEM observations (Figs. 7 and 8) suggest that the increase in the measured ΔG_0 is related to the small dislocation loops that result in the mottled dark-light contrast in Fig. 8. It should be noted that ΔG_0 is between 0.185 and 0.215 μb^3. This is of magnitude similar to what is expected for the free energy of "intermediate strength" obstacles to dislocation glide such as dislocation/dislocation interactions [10].

Table 1
dpa levels at each of the initial indentation depth, h_0 and their corresponding final indentation depths, h_f for the two kinds of irradiated samples.

h_0 (μm)	Calculated dpa at h_0 (5 dpa Zr^+ irradiated sample)	Calculated dpa at h_0 (30 dpa Zr^+ irradiated sample)	5 dpa Zr^+ irradiated sample		30 dpa Zr^+ irradiated sample	
			Avg. h_f (μm)	Approx. dpa at h_f	Avg. h_f (μm)	Approx. dpa at h_f
0.10	0.03	0.18	0.16	0.05	0.19	0.30
0.50	0.23	1.35	0.69	0.56	0.58	2.00
1.00	0.75	4.42	1.12	1.20	1.07	6.60
2.00	5.35	31.35	2.17	4.53	2.12	27.36

4. Conclusions

This paper presents the data from a study that uses pyramidal micro-indentation creep tests performed at 25 °C on non-irradiated and Zr^+ ion-irradiated Zr–2.5Nb pressure tube material to simulate the low-temperature creep deformation that drives the time-dependent blunting of scratches in CANDU reactor pressure tubes. The primary findings of this study are:

The indentation hardness (as indicated by the initial average indentation stress $\sigma_{ind,t=0}$) increased with decreasing indentation depth and increasing levels of Zr^+ ion irradiation. The depth dependence of the indentation stress is consistent with that predicted by the theories that attribute this to the increased density of geometrically necessary dislocations around sub-micrometer deep indentations.

TEM images of the indentation plastic zone in non-irradiated and ion-irradiated samples indicate that the Zr^+ ion irradiation induces regions of mottled contrast, typical of a uniform distribution of nanometer sized dislocation loops, within the microstructure. This is similar to what results from neutron irradiation. We conclude therefore that Zr^+ ion irradiation is an effective way to simulate the crystallographic damage resulting from neutron irradiation in Zr–2.5Nb.

The activation energy ΔG_0 of the obstacles that limit the rate of dislocation glide during indentation creep was assessed from the measured indentation stress and strain rates. ΔG_0 does not change with indentation depth for the non-irradiated sample and this is in agreement with what was previously reported for ΔG_0 of other ductile metals at 25 °C. ΔG_0 does however increase with increasing levels of Zr^+ ion damage and shows a non-linear relationship with dpa resulting from Zr^+ ion irradiation. The magnitude of the measured ΔG_0 is between 0.185 and 0.215 μb^3. This is similar to what is expected for the free energy of "intermediate strength" obstacles to dislocation glide such as dislocation/dislocation interactions. This suggests that the small dislocation loops shown in the TEM images of indentations made in the irradiated samples become the rate-limiting feature controlling the low-temperature creep around scratches in Zr–2.5Nb pressure tube material.

It should be noted that this study has investigated the effect of prior irradiation hardening on the kinetics of thermal creep deformation occurring, in Zr–2.5Nb, at very high stress and very low temperature. The resulting data on the effect of irradiation damage on σ_{ind} and ΔG_0 are particularly important for arriving at conservative predictions of the rate of crack tip blunting of scratches in the outboard region of a CANDU pressure tube. This research does not consider the effect of temperature and neutron flux on σ_{ind} or ΔG_0.

Acknowledgements

The authors wish to thank the Natural Science and Engineering Research Council of Canada (NSERC) and the University Network of Excellence in Nuclear Engineering (UNENE) who provided financial support for this research. The assistance of Dr. T. Simpson of the University of Western Ontario Nanofabrication Laboratory in preparing the TEM foils using focused ion beam milling is gratefully acknowledged. Finally, a special note of thanks to Dr. B. Leitch of the Atomic Energy of Canada Ltd (Chalk River Laboratories) for providing the Zr–2.5%Nb pressure tube material used in this study and providing his continuous support of this project.

References

[1] N. Christodoulou, P.A. Turner, C.N. Tomé, C.K. Chow, R.J. Klassen, Metall. Mater. Trans. A 33 (2002) 1103.
[2] A.R. Causey, A.G. Norsworthy, C.W. Schultes, Can. Metall. Quart. 24 (1984) 207.
[3] V. Bhakhri, R.J. Klassen, J. Mater. Sci. 41 (2006) 2259.
[4] V. Bhakhri, R.J. Klassen, J. Mater. Sci. 41 (2006) 2249.
[5] V. Bhakhri, R.J. Klassen, Scripta Mater. 55 (2006) 395.
[6] B. Bose, R.J. Klassen, J. Mater. Sci. Eng. A 500 (2009) 164.
[7] R.J. Klassen, B.J. Diak, S. Saimoto, Mater. Sci. Eng. A 387–389 (2004) 297.
[8] B.J. Diak, S. Saimoto, Mater. Sci. Eng. A 319–321 (2001) 909.
[9] S. Saimoto, B.J. Diak, K.R. Upadhyaya, Mater. Sci. Eng. A 234–236 (1997) 1015.
[10] H.J. Frost, M.F. Ashby, Deformation-Mechanism Maps, Pergamon Press, Oxford, 1982.
[11] U.F. Kocks, A.S. Argon, M.F. Ashby, Prog. Mater. Sci. 19 (1975) 1.
[12] W.D. Nix, H. Gao, J. Mech. Phys. Solids 46 (1998) 411.
[13] M.F. Ashby, Philos. Mag. 21 (1970) 399.
[14] Q. Ma, D.R. Clarke, J. Mater. Res. 10 (1995) 853.
[15] H. Li, A.H.W. Ngan, J. Mater. Res. 19 (2004) 513.
[16] W.J. Poole, M.F. Ashby, N.A. Fleck, Scripta Mater. 34 (1996) 559.
[17] A.A. Elmustafa, D.S. Stone, J. Mech. Phys. Solids 51 (2003) 357.
[18] M. Griffiths, J.F. Mecke, J.E. Winegar, Zirconium in the Nuclear Industry, Eleventh Int. Symp., ASTM, STP 1295, 1996, p. 580.
[19] R.A. Holt, M. Griffiths, R.W. Gilbert, J. Nucl. Mater. 149 (1987) 51.
[20] M. Griffiths, R.W. Gilbert, V. Fidleris, R.P. Tucker, R.B. Adamson, J. Nucl. Mater. 150 (1987) 159.
[21] M. Griffiths, R.W. Gilbert, C.E. Coleman, J. Nucl. Mater. 159 (1988) 405.
[22] M. Griffiths, J. Nucl. Mater. 205 (1993) 225.
[23] M. Griffiths, J. ASTM Int. 5 (2008) 1.
[24] E. Kohn, M.G. Wright, AECL Research Report, AECL-5810, 1977, p. 1.
[25] M. Griffiths, J. Nucl. Mater. 159 (1988) 190.
[26] M. Griffiths, P.H. Davis, W.G. Davis, S. Sagat, Zirconium in the Nuclear Industry, Thirteenth Int. Symp., ASTM, STP 1423, 2002, p. 507.
[27] M. Griffiths, R.C. Styles, C.H. Woo, F. Philip, W. Frank, AECL Research Report, AECL-10801, 1993, p. 1.
[28] C.D. Cann, C.B. So, R.C. Styles, C.E. Coleman, J. Nucl. Mater. 205 (1993) 267.
[29] O.T. Woo, R.M. Hutcheon, C.E. Coleman, Mater. Res. Soc. Symp. Proc. 373 (1995) 189.
[30] G.J.C. Carpenter, J.F. Watters, J. Nucl. Mater. 96 (1981) 213.
[31] C.K. Chow, R.A. Holt, C.H. Woo, C.B. So, J. Nucl. Mater. 328 (2004) 1.
[32] C. Heintze, C. Recknagel, F. Bergner, M. Hernández-Mayoral, A. Kolitsch, Nucl. Instrum. Methods Phys. Res. B 267 (2009) 1505.
[33] X.T. Zu, M. Atzmon, L.M. Wang, L.P. You, F.R. Wan, G.S. Was, R.B. Adamson, J. ASTM Int. 1 (2004) 741.
[34] V. Perovic, A. Perovic, G.C. Weatherly, L.M. Brown, G.R. Purdy, R.G. Fleck, R.A. Holt, J. Nucl. Mater. 205 (1993) 251.
[35] V. Perovic, G.C. Weatherly, R.G. Fleck, Can. Metall. Quart. 24 (1985) 253.
[36] M. Griffiths, C.K. Chow, C.E. Coleman, R.A Holt, S. Sagat, V.F. Urbanic, Atomic Energy of Canada Ltd Research Report, AECL-10844, 1993, p. 1.
[37] D. Tabor, The Hardness of Metals, Clarendon Press, Oxford, 1951. p. 105.
[38] N. Christodoulou, P.A. Turner, E.T.C. Ho, C.K. Chow, M.R. Levi, Metall. Mater. Trans. A 31A (2000) 409.
[39] A. Salinas-Rodriguez, M.G. Akben, J.J. Jonas, E.F. Ibrahim, Can. Metall. Quart. 24 (1985) 259.
[40] B.S. Rodchenkov, A.N. Semenov, Nucl. Eng. Design 235 (2005) 2009.